Osteocytes mediate the anabolic actions of canonical Wnt/β-catenin signaling in bone

Xiaolin Tu[a,1,2], Jesus Delgado-Calle[a,b,1], Keith W. Condon[a], Marta Maycas[a], Huajia Zhang[c], Nadia Carlesso[c], Makoto M. Taketo[d], David B. Burr[a], Lilian I. Plotkin[a,b], and Teresita Bellido[a,b,e,2]

[a]Department of Anatomy and Cell Biology and [e]Division of Endocrinology, Department of Medicine, Indiana University School of Medicine; [b]Roudebush Veterans Administration Medical Center and [c]Department of Pediatrics, Indiana University School of Medicine, Indianapolis, IN 46022; and [d]Department of Pharmacology, Graduate School of Medicine, Kyoto University, Kyoto 606-8501, Japan

Edited by John T. Potts, Massachusetts General Hospital, Charlestown, MA, and approved December 30, 2014 (received for review May 27, 2014)

Osteocytes, >90% of the cells in bone, lie embedded within the mineralized matrix and coordinate osteoclast and osteoblast activity on bone surfaces by mechanisms still unclear. Bone anabolic stimuli activate Wnt signaling, and human mutations of components along this pathway underscore its crucial role in bone accrual and maintenance. However, the cell responsible for orchestrating Wnt anabolic actions has remained elusive. We show herein that activation of canonical Wnt signaling exclusively in osteocytes [dominant active (da)βcat^{Ot} mice] induces bone anabolism and triggers Notch signaling without affecting survival. These features contrast with those of mice expressing the same daß-catenin in osteoblasts, which exhibit decreased resorption and perinatal death from leukemia. daßcat^{Ot} mice exhibit increased bone mineral density in the axial and appendicular skeleton, and marked increase in bone volume in cancellous/trabecular and cortical compartments compared with littermate controls. daßcat^{Ot} mice display increased resorption and formation markers, high number of osteoclasts and osteoblasts in cancellous and cortical bone, increased bone matrix production, and markedly elevated periosteal bone formation rate. Wnt and Notch signaling target genes, osteoblast and osteocyte markers, and proosteoclastogenic and antiosteoclastogenic cytokines are elevated in bones of daßcat^{Ot} mice. Further, the increase in RANKL depends on Sost/sclerostin. Thus, activation of osteocytic β-catenin signaling increases both osteoclasts and osteoblasts, leading to bone gain, and is sufficient to activate the Notch pathway. These findings demonstrate disparate outcomes of β-catenin activation in osteocytes versus osteoblasts and identify osteocytes as central target cells of the anabolic actions of canonical Wnt/β-catenin signaling in bone.

osteocytes | canonical Wnt | beta-catenin | bone anabolism | notch signaling

Bone formation by osteoblasts is coupled to bone resorption by osteoclasts. The proper balance between these two opposing processes is essential for bone health, and disruption of this balance favoring resorption causes osteopenia and eventually osteoporosis, a devastating disease that affects millions worldwide (1). Osteocytes, terminally differentiated osteoblasts embedded in the mineralized bone matrix that constitute more than 90% of all bone cells, control the generation and activity of osteoblasts and osteoclasts by mechanisms still unraveling (2, 3).

The Wnt signaling pathway has emerged as a key regulator of bone homeostasis (4). Wnt signaling controls developmental and postnatal processes including cell proliferation, differentiation, polarity, and migration through canonical and noncanonical pathways (5). β-Catenin is the obligatory transducer for canonical Wnt signaling. Upon binding to Frizzled receptors and the low-density lipoprotein receptor-related proteins (Lrp) 5 or 6, Wnt ligands stabilize β-catenin, which translocates to the nucleus and interacts with the transcription regulator Tcf/Lef to activate transcription of Wnt target genes. The importance of canonical Wnt/β-catenin (heretofore refer to as β-catenin) signaling in bone homeostasis was discovered through loss- and gain-of-function mutations in Lrp5, which induce, respectively, osteoporosis-pseudoglioma and high bone density syndromes (6–8). β-Catenin signaling exerts cell context-dependent functions on osteoblastic cells depending on the stage of differentiation. At early stages, β-catenin inactivation in mesenchymal progenitors and osteoblast-committed precursors arrests osteoblast differentiation leading to absence of bone and lack of mature osteoblasts, respectively (9–12). At later stages, however, β-catenin inactivation in mature osteoblasts/osteocytes or only in osteocytes appears not to affect osteoblast differentiation or bone formation, but instead increases osteoclast differentiation and bone resorption leading to low bone mass (13–15). Conversely, activation of β-catenin in osteoblasts leads to increased bone mass by reducing bone resorption, again without apparent effect on osteoblast production (4, 13). Further, β-catenin activation in osteoblasts induces Notch signaling-dependent alterations of hematopoiesis, leading to anemia, myeloid lineage expansion, the development of acute myeloid leukemia, and perinatal death (16).

Even when genetic manipulations of β-catenin signaling in osteoblasts alter osteoclasts and bone resorption without demonstrable effects on osteoblasts or bone formation, the pathway is linked to bone anabolism. Thus, recognized stimulators of bone formation, such as parathyroid hormone and mechanical loading, down-regulate the osteocytic Sost gene and increase β-catenin signaling (17–22). Sost encodes the protein sclerostin, a potent inhibitor of bone formation, which antagonizes Wnt

Significance

Bone anabolic stimuli activate canonical Wnt/β-catenin signaling and human mutations of this pathway underscore its essential role in bone accrual. However, the cell responsible for orchestrating these actions has remained elusive. This study identifies osteocytes as mediators of the anabolic effect of canonical Wnt/β-catenin signaling in bone; further, it dissects desired (bone gain) from undesired (decreased resorption and leukemia) outcomes by selective activation of canonical Wnt/β-catenin signaling in osteocytes versus osteoblasts. Long-lived osteocytes constitute more than 90% of bone cells, thus representing more logical and effective target cells to induce bone anabolism than scarce, short-lived osteoblasts. These findings pave the way toward the development of better treatments for osteoporosis and other bone-related disorders targeting osteocytic Wnt/β-catenin signaling.

Author contributions: X.T. and T.B. designed research; X.T., J.D.-C., K.W.C., M.M., and H.Z. performed research; M.M.T. contributed new reagents/analytic tools; X.T., J.D.-C., N.C., D.B.B., L.I.P., and T.B. analyzed data; and X.T., J.D.-C., L.I.P., and T.B. wrote the paper.

The authors declare no conflict of interest.

This article is a PNAS Direct Submission.

[1]X.T. and J.D.-C. contributed equally to this work.

[2]To whom correspondence may be addressed. Email: tbellido@iupui.edu or xiaolint@hotmail.com.

This article contains supporting information online at www.pnas.org/lookup/suppl/doi:10.1073/pnas.1409857112/-/DCSupplemental.

www.pnas.org/cgi/doi/10.1073/pnas.1409857112

signaling by binding to Lrp5/6. Lack of sclerostin expression is responsible for the high-bone-mass/high-bone-formation human diseases van Buchem and sclerosteosis (23–26). Mutations of the Lrp5 gene that render a protein unable to be inhibited by sclerostin and/or Dkk1, another Wnt antagonist, also induce high bone mass because of high bone formation (27, 28). These findings raise the possibility that the cells responsible for the anabolic outcomes of β-catenin signaling are not the less-mature cells of the osteoblastic lineage that have been targeted by the genetic manipulations. We addressed here the possibility that, instead, osteocytes, the most differentiated cells of the lineage, mediate anabolic actions of the pathway. We generated a novel osteocyte-specific knock-in mouse model expressing a dominant active (da) β-catenin in osteocytes (daβcat^{Ot}) and show that activation of β-catenin signaling in osteocytes increases bone remodeling with a positive balance in favor of bone formation resulting in bone gain. This phenomenon is due to full stimulation of osteoblast/osteocyte differentiation, leading to more bone matrix producing osteoblasts and more osteocytes, together with increased osteoclasts resulting from a Sost/sclerostin-dependent stimulation of RANKL gene expression. Further, activation of osteocytic β-catenin signaling is sufficient to enhance components of the Notch signaling pathway, but it did not alter hematopoiesis or survival. These findings demonstrate disparate outcomes of β-catenin activation in osteocytes versus osteoblasts and identify the osteocyte as a central target cell of the anabolic actions of canonical Wnt/β-catenin signaling in bone.

Results

Activation of β-Catenin in Osteocytes Increases Bone Mineral Density and Cancellous Bone Volume. Knock-in daβcat^{Ot} mice expressing dominant active β-catenin in osteocytes as demonstrated by Western blotting (Fig. 1*A*) and immunohistochemistry (Fig. 1*B* and Fig. S1*A*) exhibited up-regulation of canonical Wnt target genes compared with control littermates Catnb$^{lox(ex3)/+}$ (Fig. 1*C*). daβcat^{Ot} mice displayed no gross skeletal abnormalities at birth, as evidenced by normally formed bone and cartilage (Fig. 1*D*). After weaning, daβcat^{Ot} mice failed to grow at the same rate than littermate controls, with a 20–50% lower body weight. At 6 mo, daβcat^{Ot} mice displayed smaller body size (Fig. 1*E*) and 20% lower femoral length (12.8 ± 0.9 versus 15.9 ± 0.8 mm for littermate controls). However, no differences in growth plate thickness were found at either 2 or 4 mo of age (Fig. 1*I* and Fig. S2). Circulating PTH was increased and calcium was decreased in 2-mo-old daβcat^{Ot} mice, but both were normal in 4-mo-old mice (Fig. S3*A*). No changes in phosphate were detected.

Longitudinal analysis showed progressive increase in bone mineral density (BMD) in daβcat^{Ot} mice compared with controls (Fig. 1*F*). At 4 mo of age, both female and male daβcat^{Ot} mice exhibited a similar increase in total, spinal, and femoral BMD (Fig. 1*G*). X-ray radiography showed denser femoral, tibial, and vertebral bones in daβcat^{Ot} mice compared with controls (Fig. 1*H*). Von Kossa or Goldner's trichrome staining showed more mineralized bone in the distal femur of daβcat^{Ot} mice (Fig. 1*I* and Fig. S2 *B* and *C*). Microcomputed tomography (μCT) analysis of the distal femur revealed more cancellous bone (Fig. 1*J*) and increased bone volume and trabecular number by eightfold and sixfold, respectively, and markedly decreased trabecular separation, and increased trabecular thickness at 4 mo of age (Fig. 1*K*). Histomorphometric analysis confirmed these findings at both 2 and 4 mo of age, albeit trabecular thickness was not increased (Fig. 1*L*).

Osteocytic Activation of β-Catenin Unexpectedly Increases Bone Resorption. Although eruption of the lower incisors was not complete, daβcat^{Ot} mice exhibited full eruption of upper incisors and molars (Fig. 2*A*) and displayed a threefold and twofold increase in circulating levels of C-telopeptide fragments of type I collagen (CTX), a marker of bone resorption, at 2 and 4 mo of age, respectively, compared with control littermates (Fig. 2*B*). Abundant osteoclasts were found in bones of daβcat^{Ot} mice, as detected by osteoclast-specific TRAPase staining and quantified for both 2- and 4-mo-old mice (Fig. 2 *C*–*F*). In cancellous bone of the distal femur, osteoclast number per tissue area was increased by two- to threefold in daβcat^{Ot} mice compared with controls (Fig. 2*C*). However, osteoclast number and surface normalized per bone surface was not different between genotypes, likely due to the remarkable increase in cancellous bone surface in the daβcat^{Ot} mice. On the femoral endocortical surface, osteoclast number and surface were also markedly increased by sixfold and eightfold, respectively, but only at 4 mo of

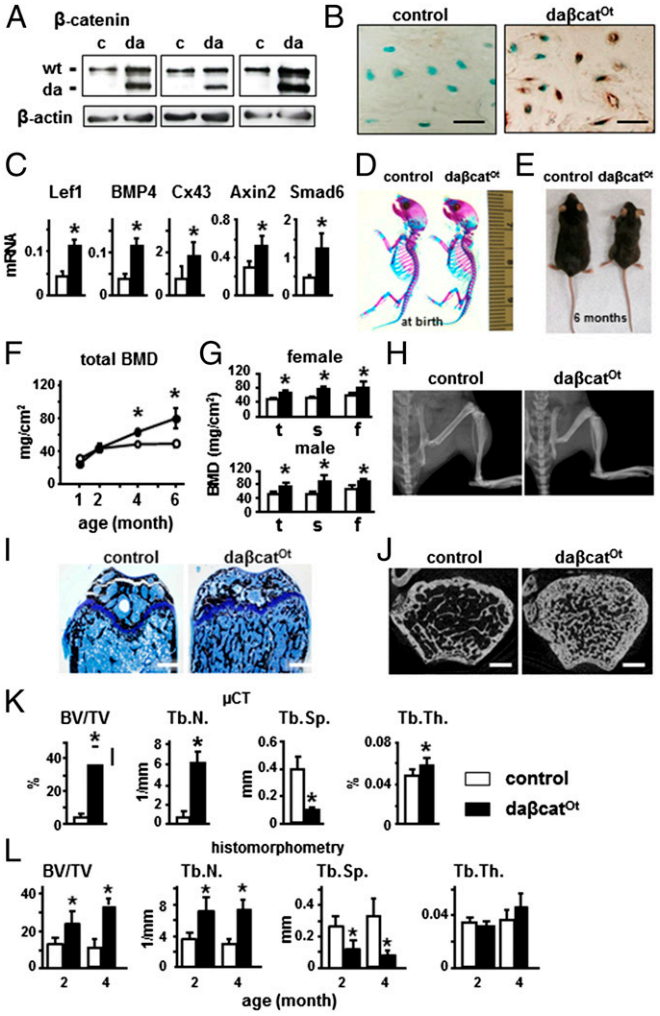

Fig. 1. Osteocytic activation of β-catenin increases Wnt signaling in bone, and elevates bone mineral density and cancellous bone volume. (*A*) Western blotting for dominant active (da) and wild-type (wt) β-catenin in long bone lysates of control (c) and daβcat^{Ot} (da) mice (2-mo-old). (*B*) Immunohistochemistry for β-catenin in osteocytes from distal femur. (*C*) qPCR for canonical Wnt target genes using lumbar vertebrae (L4) mRNA (2-mo-old). *$P < 0.05$ by *t* test, $n = 6$–9 mice. (*D*) Whole-mount skeletal staining of newborn pups; bone (red) and cartilage (blue). Ruler in millimeters. (*E*) Control and daβcat^{Ot} male mice (6-mo-old). BMD of female mice (*F*) and of male and female mice (4-mo-old) (*G*). *$P < 0.05$ by two-way ANOVA, $n = 7$–10 mice. f, femoral; s, spinal; t, total. (*H*) X-rays of hindlimbs. (*I*) Von Kossa/Toluidine blue staining of distal femur longitudinal sections from 4-mo-old mice. (*J*) Representative μCT cross-sectional reconstructed images of distal femur of 4-mo-old mice. BV/TV, and trabecular number (Tb.N.), separation (Tb.Sp.), and thickness (Tb.Th.) were measured by μCT in 4-mo-old mice (*K*) and histomorphometry in 2- and 4-mo-old mice (*L*). *$P < 0.05$ by *t* test, $n = 4$ mice. (Scale bars: *B*, 25 μm; *H*, 2 mm; *I* and *J*, 0.5 mm.)

age (Fig. 2 *D* and *E*). Further, osteoclasts were increased within cortical bone from daβcat^{Ot} mice at 2 or 4 mo of age (Fig. 2*F*). This effect led to 21-fold and 35-fold increases in intracortical porosity compared with control littermates at 2 and 4 mo of age, respectively (Fig. 2*F*). No difference between genotypes was

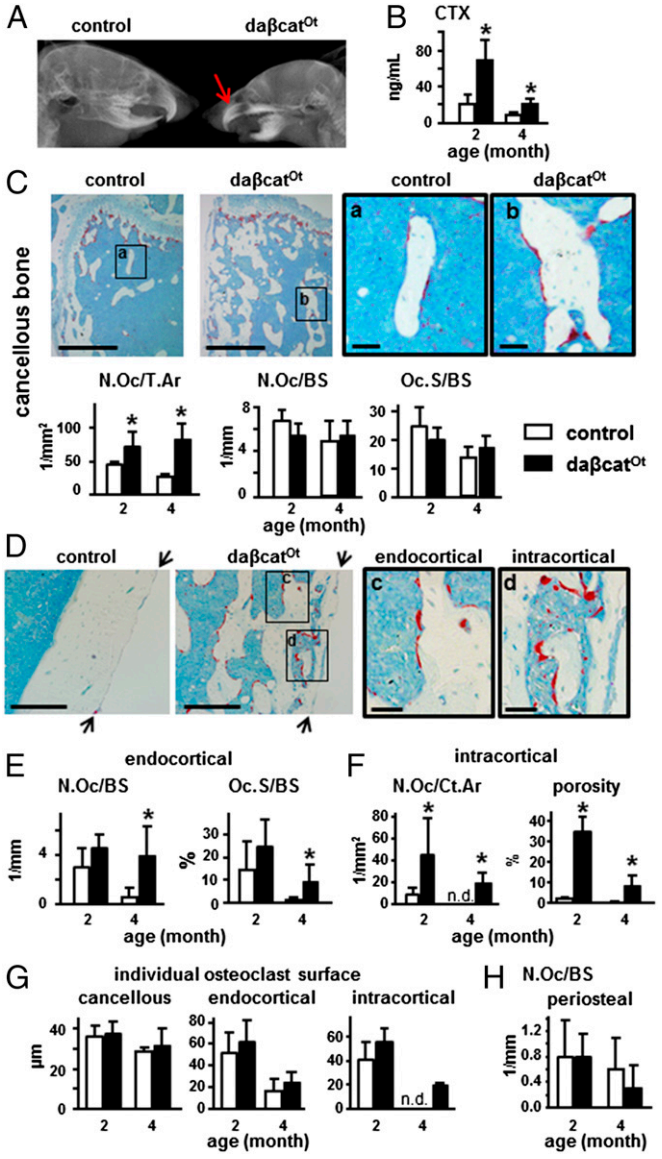

Fig. 2. Osteocytic activation of β-catenin increases bone resorption. (*A*) X-ray of the head showing eruption of upper incisors (red arrow) in daβcat^{Ot} mice (1-mo-old). (*B*) Plasma CTX levels, $n = 8$–14 mice. *$P < 0.05$ by *t* test. (*C*–*H*) Histomorphometric quantification of TRAPase-stained osteoclasts in longitudinal sections of distal femur (2- and 4-mo-old mice). (*C*) Microscopy images of osteoclasts on cancellous bone of 4-mo-old mice. Areas *a* and *b* are magnified on the right. Osteoclast number normalized to tissue area (N.Oc/T.Ar) or to bone surface (N.Oc/BS), and osteoclast surface normalized to bone surface (Oc.S/BS). (*D*) Microscopy images showing osteoclasts on endocortical and intracortical bone surfaces of distal femur of 4-mo-old mice. Arrows point at periosteal surface. Areas *c* and *d* are magnified on the right. (*E*) Endocortical osteoclast number (N.Oc) and surface (Oc.S) normalized by bone surface (BS). (*F*) Intracortical osteoclast number normalized to cortical bone area (N.Oc/Ct.Ar) and percent porosity. (*G*) Average surface occupied by individual osteoclast on cancellous, endocortical, and intracortical bone. (*H*) Osteoclast number on periosteal bone surface (N.Oc/BS). *$P < 0.05$ by *t* test, $n = 3$ mice for (C–*H*). (Scale bars: *C, Left*, 0.5 mm; *C, Right*, 0.1 mm; *D, Left*, 0.2 mm; *D, Right*, 0.05 mm.)

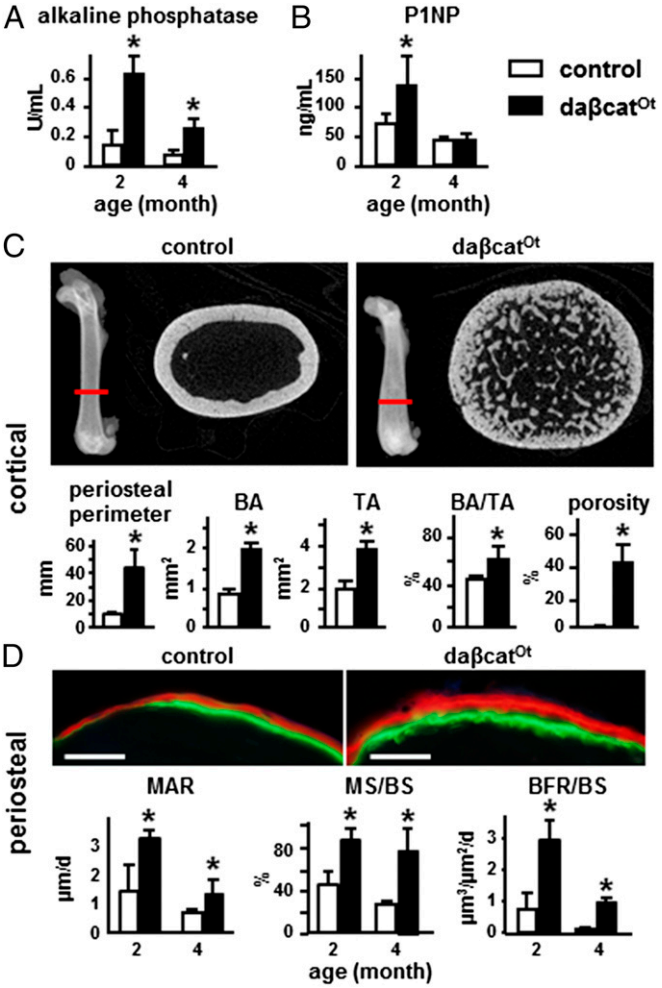

Fig. 3. Osteocytic activation of β-catenin increases periosteal bone formation and cortical bone. (*A* and *B*) Plasma levels of alkaline phosphatase and P1NP, $n = 8$–11 mice; *$P < 0.05$ by *t* test. (*C*) Representative reconstructed μCT images of cross-sectional femoral bone at the location indicated with the red line (4-mo-old). Periosteal perimeter, bone area (BA), tissue area (TA), BA/TA, and cortical porosity are shown. (*D*) Dynamic histomorphometric analysis on periosteal bone surfaces. Representative images of fluorochrome incorporation at the periosteal surface. (Scale bars: 0.1 mm.) BFR/BS, bone formation rate per bone surface; MAR, mineral appositional rate; MS/BS, percent mineralizing bone surface per bone surface. *$P < 0.05$ by *t* test, $n = 7$ mice per genotype.

detected in the surface of individual osteoclasts (Fig. 2*G*), or in the number of osteoclasts on the periosteal surface (Fig. 2*H*). The increased resorption exhibited by daβcat^{Ot} mice contrasts with the previously reported phenotype of mice expressing the same daβ-catenin in osteoblasts using the Col1-2.3kb-Cre mice, which lack tooth eruption, die after weaning, and exhibit low bone resorption and osteopetrosis (13).

Osteocytic Activation of β-Catenin Increases Cortical Bone, Osteoblast Number, and Bone Formation. The osteoblast marker alkaline phosphatase was increased in plasma of both 2- and 4-mo-old mice (Fig. 3*A*). Procollagen type 1 amino-terminal propeptide (P1NP), a bona fide bone formation marker, was also elevated in 2-mo-old mice (Fig. 3*B*). μCT showed more bone in cross-sections at the femoral diaphysis with enlarged diameter in daβcat^{Ot} mice compared with controls at 4 mo (Fig. 3*C*). Quantification demonstrated an increase of 4.7-, three-, and twofold in periosteal perimeter, cortical bone area and tissue area, resulting in

increased BA/TA (Fig. 3*C*). Consistent with the findings in the distal femur (Fig. 2*F*), daßcat^{Ot} mice also exhibited a remarkable 150-fold increase in cortical porosity at the femoral diaphysis (Fig. 3*C*).

Dynamic bone histomorphometric analysis demonstrated higher bone formation rate (BFR/BS) on the periosteal surface at both 2 and 4 mo of age (Fig. 3*D*). This effect resulted from combined higher mineral appositional rate (MAR) and mineralizing surface per bone surface (MS/BS), reflecting increased individual osteoblast activity and more osteoblasts covering the bone surface, respectively.

Consistent with the elevated bone formation on the periosteal surface, osteoblast number per tissue area was increased in cancellous bone (Fig. 4*A*) and on the femoral endocortical surface (Fig. 4*B*) of daßcat^{Ot} mice at 2 and 4 mo of age. In contrast to the periosteal surface, however, dynamic histomorphometric analysis failed to demonstrate greater BFR on these surfaces. Instead, in cancellous bone, BFR/BS was not changed at 2 mo of age but was lower at 4 mo of age because of lower MAR (Fig. S4*A*). On the endocortical surface, MAR is lower at both 2 and 4 mo, and MS/BS is lower at 4 mo; consequently, BFR/BS is lower at both time periods. It is possible that the significantly lower endocortical MS/BS at 4 mo is due to the higher N.Oc/BS and Oc.S/BS that occurs at 4 mo but is not present at 2 mo (Fig. S4*B*). At 4 mo of age for cancellous surfaces and at both ages for the endocortical surface, reduced BFR was associated with significantly less surface covered by double labels and more single-labeled surface (Fig. S4 *C* and *D*). In addition, there was a preferential loss of the first (green) label compared with the second (red) label on both bone surfaces at 4 mo of age (Fig. S4*E*). Moreover, both green and red labels displayed considerable thinning compared with the strongly fluorescent and wide labels exhibited by the littermate controls (Fig. S4 *C* and *D*). However, bone matrix formation was not impaired, as demonstrated by the marked accumulation of osteoid revealed with two special staining procedures that discriminate nonmineralized from mineralized bone matrix (Fig. 4*C* and Fig. S2 *B* and *C*). Quantification of von Kossa-stained sections showed a marked increase in osteoid volume in cancellous bone of the distal femur and cortical bone of the diaphysis, at 2 and, to a lesser extent, at 4 mo of age (Fig. 4*C* and Fig. S3*B*). More osteoid together with lower MAR resulted in elevated mineralization lag time on cancellous surfaces at 2 mo, and on the endocortical surface at both ages (Fig. 4*D*). Further, osteocyte density was increased at both ages in the cancellous compartment and the diaphysis (Fig. 4*E*). In contrast, neither osteoid volume nor osteocyte density was different from controls in the cortical bone of the distal femur (Fig. 4 *C* and *E* and Fig. S3*B*). The combination of increased resorption and accumulation of osteoid explains the lack of increased BMD at 2 mo of age, even when circulating P1NP, periosteal BFR, and cancellous/endocortical osteoblast number and osteoid volume are increased. At 4 mo of age, the increase in osteoid volume in daßcat^{Ot} mice lessened, demonstrating that osteoid eventually mineralizes. Accordingly, BMD at 4 mo is higher than in controls and the difference in BMD accentuates at 6 mo of age (Fig. 1 *F* and *G*).

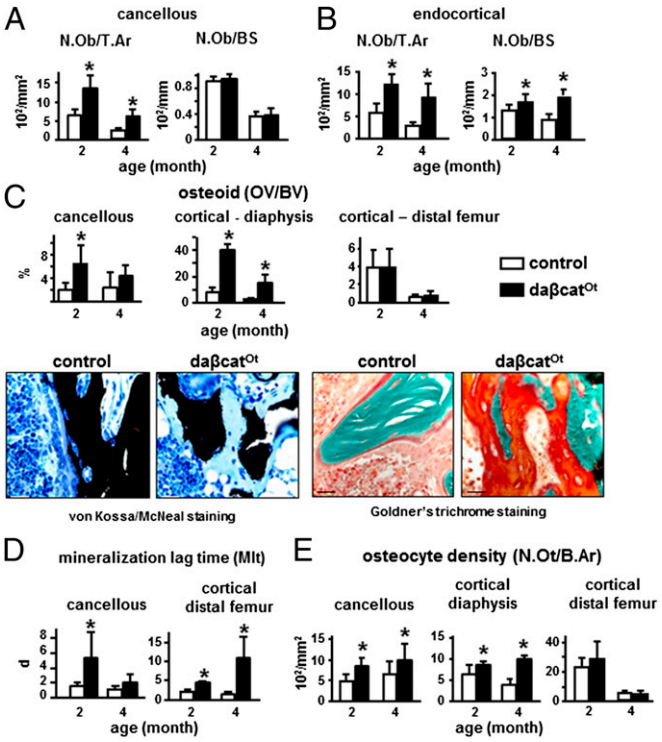

Fig. 4. Osteocytic activation of β-catenin increases osteoblast number, osteoid production, and osteocyte density in cancellous and cortical bone. Static histomorphometric analysis was performed in femoral cancellous and cortical bone of 2- and 4-mo-old mice. (*A* and *B*) Osteoblast number per tissue area (N.Ob/T.Ar) and per bone surface (N.Ob/BS). (*C*) Osteoid volume per bone volume (OV/BV) and representative images of longitudinal sections of femoral bone stained by von Kossa/McNeal (bone black and osteoid light blue) or Goldner's trichrome (bone green and osteoid orange/red) to discriminate mineralized bone from osteoid are shown. (Scale bars: 25 μm.) (*D*) Mineralization lag time calculated as osteoid thickness divided by MAR. (*E*) Osteocyte density (N.Ot/B.Ar), $^*P < 0.05$ by *t* test, $n = 7$ mice per genotype.

Osteocytic Activation of β-Catenin Signaling Increases Osteoblast/Osteocyte Differentiation and Proosteoclastogenic Cytokine Expression. No changes in the proliferation marker PCNA or in the prevalence of osteoblast apoptosis were detected (Fig. S3 *C* and *D*). In contrast, and consistent with the tissue and cellular phenotype, markers of osteoblasts and osteocytes were elevated in bones of daßcat^{Ot} mice. Expression of the osteoblast transcription factors Runx2 and Osterix, as well as alkaline phosphatase and osteocalcin, was increased with no changes in collagen 1 (Fig. 5*A*), and expression of the osteocyte marker Sost and of DMP1, Dkk1, and MEPE expressed by osteoblasts and osteocytes was also elevated (Fig. 5*B*). This evidence combined with the higher osteocyte density (Fig. 4*E*) indicates that osteoblasts differentiate faster to produce more osteocytes. Further, the prevalence of sclerostin-positive osteocytes is higher in all bone envelopes of the daßcat^{Ot} mice compared with controls (Fig. 5*C* and Fig. S1*B*), even in the diaphysis in which approximately one-half of the bone is not mineralized (osteoid) (Fig. 4*C*). Because sclerostin is a marker of fully differentiated osteocytes embedded in mineralized bone, this evidence is consistent with accelerated osteocyte maturation.

Similar to mice with β-catenin activation in osteoblasts/osteocytes (13), OPG expression in daßcat^{Ot} mice was higher than controls (approximately fourfold) (Fig. 5*D*). However, RANKL expression was even higher (>ninefold), resulting in increased RANKL/OPG ratio. The expression of the mitogen for osteoclast precursors macrophage colony stimulating factor (M-CSF) was also elevated. Increased M-CSF and RANKL/OPG ratio explain the elevated osteoclasts and bone resorption exhibited by daßcat^{Ot} mice. mRNA expression of the osteoclast markers cathepsin K (Ctsk), TRAP, calcitonin receptor, and RANK was not changed or even decreased in bones from daßcat^{Ot} mice of the axial and appendicular skeleton at both 2 and 4 mo of age (Dataset S1). Because abundant TRAP-positive osteoclasts are detected in bone and CTX is increased in the circulation, this paradox could be explained by the fact that the cellular population in the daßcat^{Ot} bones is dominated by osteocytes/osteoblasts masking the increase in osteoclastic gene expression.

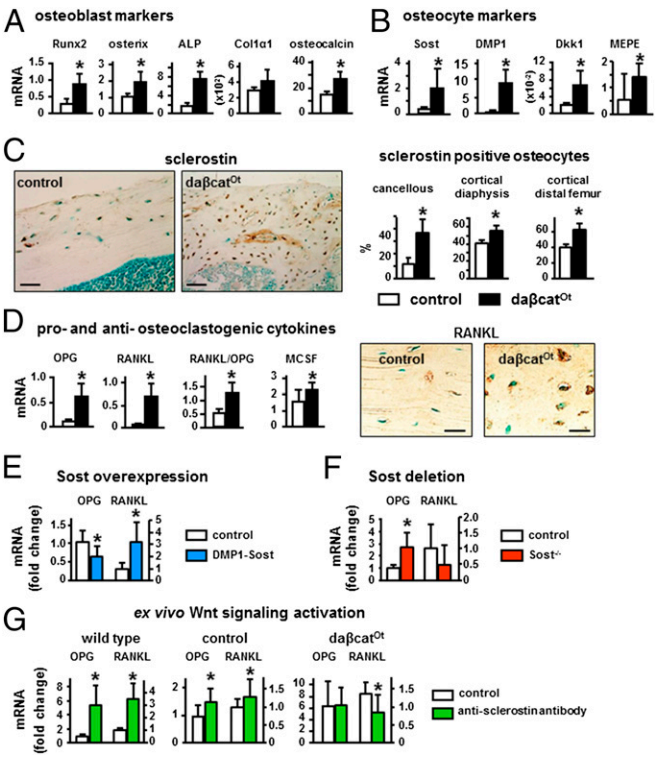

Fig. 5. Osteocytic activation of β-catenin increases osteoblast and osteocyte markers and proosteoclastogenic and antiosteoclastogenic cytokines. (*A, B,* and *D*) Gene expression was quantified by qPCR in lumbar vertebrae (L4) (2-mo-old). $*P < 0.05$ by *t* test, $n = 6–9$ mice. (*C*) The percentage of sclerostin-positive osteocytes was quantified in longitudinal sections of femoral bone stained with an anti-sclerostin antibody. $*P < 0.05$ by *t* test, $n = 3$ mice. RANKL protein expression was detected by immunohistochemistry in longitudinal sections of distal femur of 4-mo-old mice. (*E* and *F*) OPG and RANKL expression in mice overexpressing or lacking the Sost gene. (*G*) OPG and RANKL expression induced by Wnt activation by treating bones from 5-wk-old wild type or 3-wk-old controls and daβcat^{Ot} mice with an anti-sclerostin antibody. (Scale bars: *C*, 50 μm; *D*, 25 μm.)

To address the possibility that activation of β-catenin in osteocytes increases RANKL via a Sost/sclerostin-dependent mechanism, RANKL expression was analyzed in mouse models with altered Sost expression. DMP1-Sost transgenic mice overexpressing Sost in osteocytes exhibited increased RANKL expression, and the expected decreased in the expression of OPG and other Wnt target genes (22) (Fig. 5*E*). Furthermore, Sost knockout mice exhibited the expected increase in OPG but no changes in RANKL expression (Fig. 5*F*). These results demonstrate that Sost overexpression is sufficient to increase RANKL, and it is needed to increase RANKL by Wnt activation. Moreover, as in vivo in the daβcat^{Ot} mice, activating Wnt signaling ex vivo (by blocking secreted sclerostin with a neutralizing antibody; ref. 29) increased mRNA expression for OPG and RANKL in bone organ cultures from WT mice or from control Catnb$^{lox(ex3)/+}$ mice (Fig. 5*G*). However the anti-sclerostin antibody did not alter the already elevated expression of OPG but reversed to control levels the increased expression of RANKL in bones from daβcat^{Ot} mice, demonstrating that increased RANKL induced by osteocytic activation of β-catenin requires sclerostin function. Taken together, these findings demonstrate that β-catenin activation increases OPG in all cells of the osteoblastic lineage, whereas it only increases RANKL in osteocytes that also express Sost/sclerostin.

Notch Signaling Lies Downstream of β-Catenin Activation in Osteocytes. Cross-talk between the Wnt and Notch signaling pathways has been shown through the regulation of Notch ligands by β-catenin signaling (30–33). Consistent with this evidence, bones of daβcat^{Ot} mice exhibited higher levels of mRNA expression for Notch ligands, Notch receptors, and Notch target genes (Fig. 6 *A–C* and Dataset S1). Although slight changes in the gene expression profile were found at 2 versus 4 mo of age and in bones of the axial or appendicular skeleton, overall mRNA expression of all components of the Notch signaling pathway was increased in daβcat^{Ot} mice. Moreover, the expression of the Notch target gene Hes 1 at the protein level was increased in osteocytes in long bones (Fig. 6*D*).

In contrast to recent findings in mice with β-catenin activation in osteoblasts that exhibit Jag1-dependent expansion of myeloid cells leading to leukemia, anemia, and perinatal death (16), the increased Notch ligand/receptor/target gene expression induced by osteocytic activation of β-catenin did not cause premature death (Fig. 6*F*) or splenomegaly, with only minimal changes in spleen weight (Fig. 6*G*). Moreover, hematocrit and the number of red blood cells were normal (Fig. 6*H*); there was no thrombocytopenia and, instead, platelet number was slightly increased (Fig. 6*I*). Further, no changes were found in the overall white blood cell count, or in the number of neutrophils, lymphocytes, or monocytes (Fig. 6*J*). Thus, daβcat^{Ot} mice do not exhibit hematological changes consistent with anemia or leukemia in young (1.5-mo-old) or adult (4-mo-old) mice.

Discussion

Bone anabolic stimuli activate canonical Wnt/β-catenin signaling, and human mutations of components along this pathway underscore its crucial role in bone accrual and maintenance by stimulating bone formation. Paradoxically, however, genetic activation of β-catenin signaling in bone forming osteoblasts and their progenitors decreases osteoclasts and bone resorption, without apparent effects on bone formation. The current study demonstrates that, in contrast, activation of this pathway exclusively in osteocytes—terminally differentiated cells of the osteoblastic lineage—is sufficient to induce bone anabolism. These findings identify the osteocyte as a central target cell of the bone anabolic actions of β-catenin signaling. Because osteocytes are long-lived and constitute more than 90% of bone cells, they represent a more-effective target than scarce, short-lived osteoblasts, in the quest toward the development of better treatments for osteoporosis and other bone-related disorders.

The findings reported here challenge the current paradigm that β-catenin signaling in osteoblastic cells only regulates bone resorption, without affecting bone formation (13–15). Mice lacking β-catenin in osteoblast precursors, osteoblasts, or osteocytes, indeed, display severe osteopenia because of decreased OPG and exacerbated bone resorption (13–15, 34). However, MAR and BFR are decreased upon conditional deletion of β-catenin from osteoblast precursors in 2-mo-old mice (34). In addition, mice with β-catenin haploinsufficiency in osteocytes display a defective anabolic response to bone loading (35). These pieces of evidence have suggested a role for β-catenin signaling in osteoblastic cells controlling osteoblast activity. However, a direct demonstration of bone anabolism was missing. The current report demonstrates that β-catenin activation selectively in osteocytes leads to bone gain, proving that osteocytes are the cells of the osteoblastic lineage that enable bone anabolism in response to β-catenin signaling. These findings strongly suggest that osteocytes also might mediate anabolism induced by systemic activation of the pathway, with inhibitors of GSK3β or neutralizing antibodies of sclerostin, or even in human mutations of components of the Wnt pathway (4). The fact that osteocytes comprise most of the cells in bone might explain why bone anabolism is the most patent outcome of systemic Wnt activation,

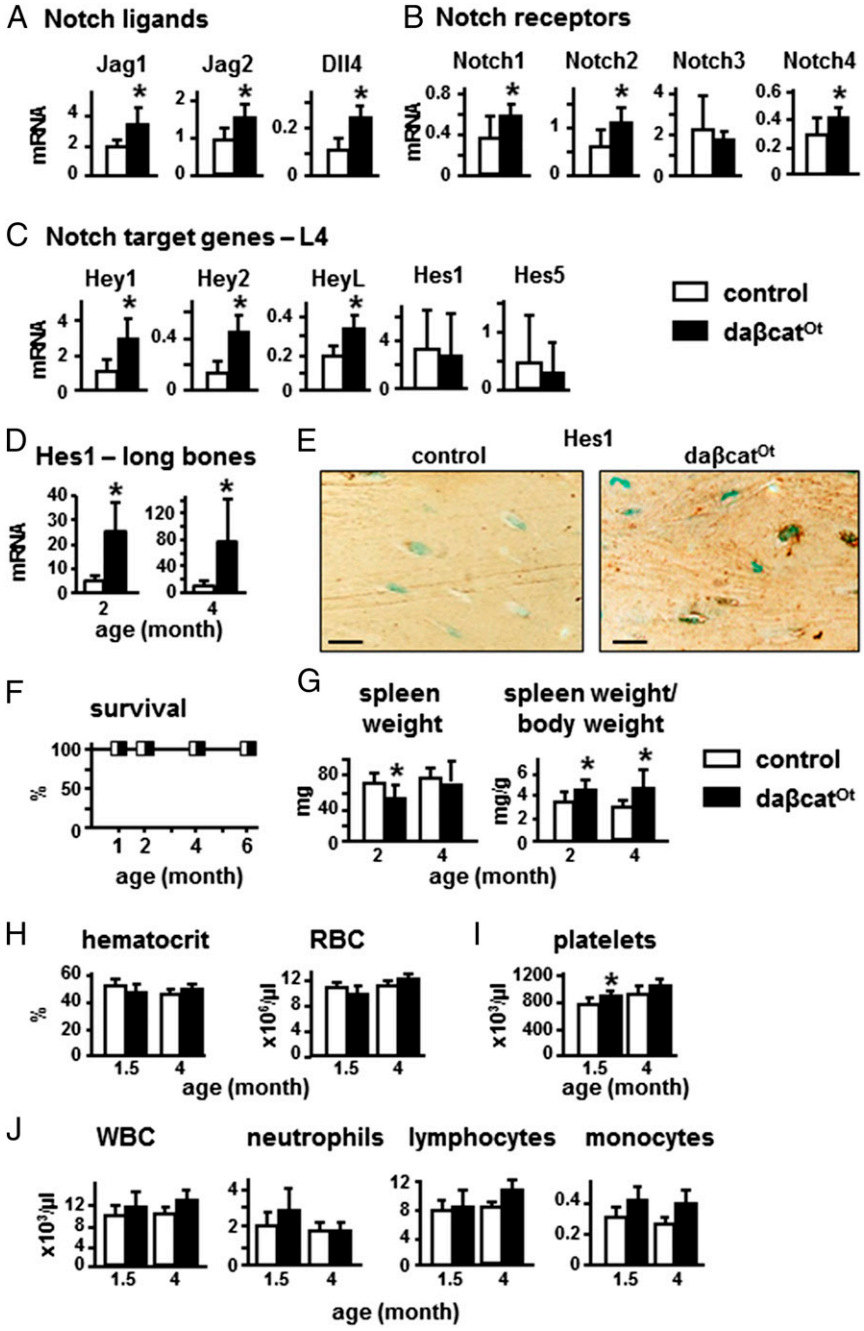

Fig. 6. Osteocytic activation of β-catenin increases expression of ligands, receptors, and target genes of the Notch pathway, without affecting hematopoiesis or life span. (*A–D*) Gene expression was quantified in lumbar vertebrae (L4) or long bones from 2- and 4-mo-old mice; $n = 6–9$ mice. (*E*) Hes 1 protein expression was detected by immunohistochemistry in longitudinal sections of distal femur of 4-mo-old mice. (Scale bars: 25 μm.) (*F*) Mouse survival rate up to 6 mo of age; $n = 7–10$ mice. (*G*) Spleen weights (2- and 4-mo-old). (*H–J*) Hematocrit and peripheral blood cell number (1.5- and 4-mo-old mice); $n = 6–8$. $^*P < 0.05$ by *t* test.

even when inhibition of resorption might be also manifested in some instances (36).

Our findings also established unexpected facts regarding the control of resorption by the β-catenin pathway. daβcat^{Ot} mice exhibit tooth eruption, increased osteoclasts, and elevated resorption. This aspect of the phenotype contrasts with the findings in mice expressing the same dominant active β-catenin in osteoblasts, which lack tooth eruption and exhibit reduced resorption. Therefore, activation of β-catenin signaling in osteocytes versus in less mature cells of the osteoblastic lineage leads to opposite effects on resorption. Whereas in both cases OPG expression is increased, in daβcat^{Ot} mice, RANKL expression is even higher, resulting in elevated RANKL/OPG ratio. Previous studies showed no changes in RANKL expression by either deletion or activation of β-catenin in Col1-2.3kb–expressing cells or activation of the pathway in osteocalcin-expressing cells in vivo (13). Hence, a major difference between β-catenin activation in osteocytes with these other models is the increased RANKL. Further, we demonstrate now that increased RANKL is a consequence of increased Sost expression in daβcat^{Ot} mice. Several pieces of evidence support this mechanism. Overexpression of Sost is sufficient to elevate RANKL expression, whereas Wnt signaling

activation fails to increase RANKL in mice lacking the Sost gene. Similar to these in vivo findings, activation of Wnt signaling ex vivo enhances RANKL expression; furthermore, the increased RANKL expression in bones from daßcat^{Ot} mice is abolished by an anti-sclerostin antibody. Therefore, taken together with previous studies (13, 14), our findings demonstrate that β-catenin activation increases OPG in all cells of the osteoblastic lineage, whereas it only increases RANKL in osteocytes that also express Sost. Our results are consistent with earlier studies demonstrating that elevated expression of Sost/sclerostin up-regulates RANKL (19, 37) and increases osteoclasts (37). Expression of M-CSF is also elevated in daßcat^{Ot} mice, consistent with our recent findings demonstrating that M-CSF is a downstream target of RANKL in osteocytes (38). Thus, the combination of elevated RANKL and M-CSF prevails over the increased expression of OPG, and resorption is then elevated in daßcat^{Ot} mice. Comparison of the phenotype of daßcat^{Ot} mice with that of mice in which β-catenin was deleted from osteocytes (15) revealed another unforeseen finding that both activation and deletion of β-catenin in osteocytes leads to increased bone resorption. Expectedly, the canonical Wnt/β-catenin target gene OPG is regulated in the opposite manner in the two models, because its expression is increased by activation and decreased by deletion of β-catenin in osteocytes. However, whereas low OPG leads to increased resorption with deletion of β-catenin, high OPG resulting from activation of the pathway is surmounted by the even higher levels of RANKL and M-CSF, and then resorption is also increased.

More osteoclasts in daßcat^{Ot} mice might explain the paradoxical low MS/BS and BFR in the presence of more osteoblasts on endocortical bone surfaces. The loss of double labels and the presence of abundant, thin labels might be due to bone being resorbed shortly after it is formed. Consistent with this hypothesis, greater BFR could be readily detected on the periosteal surface where there were not more osteoclasts. Further, low MAR in the context of osteoid overproduction leads to longer mineralization lag time and indicates a mismatch between the high rate of bone matrix production and the relative low rate of mineralization. Nevertheless, the accumulated osteoid eventually mineralizes, resulting in a progressive increase in BMD.

Similar high bone mass and high bone turnover phenotype is found in mice with activation of the PTH receptor in osteocytes (18, 19, 38–40). Remarkably, however, the mechanisms underlying the skeletal phenotypes of these two mouse models are diametrically opposite. Indeed, with osteocytic PTH receptor activation, Sost/sclerostin expression is decreased, whereas with osteocytic β-catenin activation, Sost/sclerostin expression is increased. Because Sost/sclerostin and OPG are both increased instead of being decreased as expected with PTH elevation, it is unlikely that the increased PTH levels found in 2-mo-old mice contribute to the skeletal phenotype of the daßcat^{Ot} mice.

Notch signaling is activated by cell-to-cell communication between membrane-bound ligands and receptors. Previous studies in other cell types suggested that Notch activation lies downstream of Wnt signaling (30–33). The present study demonstrates that also in osteocytes, activation of β-catenin signaling is sufficient to trigger Notch activation and to increase the expression of traditional Notch target genes. The expression of the ligands Jag1 and 2 and Dll4, and the receptors Notch 1, 2, and 4 is also elevated in daßcat^{Ot} mice, raising the possibility that osteocytic β-catenin initiates a chain of Notch activation throughout the osteocyte network, by which signals are amplified in an autocrine/paracrine fashion. Earlier studies demonstrated that the effects of Notch signaling in the skeleton are complex and, similar to Wnt signaling, are cell-context specific and dependent on the stage of osteoblastic cell differentiation (41–44). In particular, activation of Notch signaling in osteocytes has a strong impact on bone homeostasis, by mechanisms still unclear and which appear to be different in cancellous versus cortical bone (45). Mice with osteocytic activation of Notch exhibit increased cancellous bone and elevated resorption with exacerbated porosity in cortical bone (45). These features resemble the ones exhibited by daßcat^{Ot} mice, raising the possibility that Notch activation is responsible for some of the skeletal consequences of activating osteocytic β-catenin.

β-Catenin activation in osteoblasts affects not only the skeleton, but also induces anemia and expansion of myeloid cells, leading to leukemia and premature death by 6 wk of age (16). This effect results from increased expression of Jag1 in osteoblasts, which triggers Notch signaling in hematopoietic stem cell progenitors. In contrast to these findings, daßcat^{Ot} mice do not exhibit hematological changes consistent with anemia or leukemia, suggesting that in this case the elevated expression of Jag1 (and the other Notch ligands) does not activate Notch signaling in cells of the hematopoietic lineage. The inability of Notch ligands expressed in osteocytes to activate Notch signaling in hematopoietic cells might be explained by the relatively restricted access of osteocytes compared with osteoblasts to direct cell-to-cell contact with hematopoietic cells under physiological conditions. In contrast, osteocyte-osteocyte contact within the lacunar-canalicular network provides the basis for Notch activation in osteocytes themselves, as evidenced by increased expression of Hes 1. Future studies, outside the scope of the current work, are warranted to clarify the mechanism underlying the differential target cells of Notch activation induced by constitutive activation of β-catenin along the osteoblastic lineage.

The consequences of Sost up-regulation for bone anabolism observed in daßcat^{Ot} mice are not fully understood. However, elevated Sost/sclerostin expression might temper the anabolic response in older mice to protect them from excessive bone gain. In fact, the increase in circulating P1NP, periosteal bone formation, and osteoid volume in daßcat^{Ot} mice is smaller at 4 mo of age than at 2 mo of age. A similar mechanism recently has been proposed for the attenuation of the anabolic response to administration of an anti-sclerostin antibody (46).

β-Catenin is the molecular mediator of canonical Wnt signaling, thus examining the consequences of its activation is a powerful approach to uncover the role(s) of canonical Wnt signaling in osteocytes. However, it is important to note that our model is not entirely equivalent to activation of canonical Wnt signaling by a ligand, which would also activate receptor-mediated events upstream of β-catenin and trigger the pathway in other cells besides osteocytes. Further, our model also differs from signal transduction activated by Wnt ligands, which might involve canonical and noncanonical signaling pathways.

In conclusion, our study dissects desired (bone gain) from undesired (decreased resorption and leukemia) outcomes by selective activation of canonical Wnt/β-catenin signaling in osteocytes versus osteoblasts.

Materials and Methods

Mice. daßcat^{Ot} mice were generated by crossing DMP1-8kb-Cre mice, which express Cre recombinase in osteocytes, but not in osteoblasts (47), with Catnb$^{lox(ex3)}$ mice, in which exon 3 that encodes for the sites required for β-catenin degradation is flanked by LoxP sites (48). Hemizygous DMP1-8kb-Cre$^{+/-}$ mice were crossed with homozygous Catnb$^{lox(ex3)/lox(ex3)}$ mice. The cross rendered 50% Catnb$^{lox(ex3)/+}$;DMP1-8kb-Cre$^{+/-}$ (named daßcat^{Ot} mice) and 50% controls Catnb$^{lox(ex3)/+}$ mice. Generation and characterization of DMP1-8kb-Cre mice was published (47). DMP1-8kb-Cre mice are of C57BL/6 background, are born at the expected Mendelian frequency, both males and females are fertile, and exhibit normal size and weight. DMP1-8kb-Cre mice are maintained as hemizygous (DMP1-8kb-Cre$^{+/-}$). The skeletal phenotype of the DMP1-8kb-Cre mice is indistinguishable from the wild-type C57BL/6 mice or from the Catnb$^{lox(ex3)/+}$ mice used as littermate controls in the current study. Mice were fed with wet regular diet (Harlan), received water ad libitum, and were maintained on a 12-h light/dark cycle. All animal procedures were approved by the Institutional Animal Care and Use Committee of Indiana University School of Medicine.

Analysis of Skeletal Phenotype. Radiographs of mouse skeleton were generated by using a Pixarray 100 (Bioptics) with 1-s exposure under 45 kV. BMD measurement and micro-CT analysis were performed as described (19, 22). Mice were anesthetized via inhalation of 2.5% (vol/vol) isoflurane (Abbott Laboratories) mixed with O_2 (1.5 L/min), and BMD of the total body, excluding the head and the tail, the lumbar spine (L1–6), and the femur was measured by dual energy X-ray absorptiometry (DXA) by using a PIXImus II densitometer (GE Medical Systems) in mice at 1, 2, 4, and 6 mo of age. For micro-CT analysis, bones from 4-mo-old mice were dissected, cleaned off soft tissue, fixed in 10% buffered formalin, and stored in 70% ethanol until scanned at 6-μm resolution (Skyscan 1172; SkyScan).

Serum Biochemistry. Plasma was obtained from blood from the facial vein of mice after 3-h fasting at the indicated age. P1NP and CTX were measured by using ELISA kits (Biomedical Technologies and Immunodiagnostic Systems), respectively (41, 42, 49). Alkaline phosphatase was measured on a Randox Daytona analyzer (Randox Laboratories Limited) at the General Clinical Research Center of Indiana University School of Medicine. Parathyroid hormone levels were measured in plasma by using a mouse PTH 1–84 ELISA Kit (Immunotopics). Calcium measurement was performed at the General Clinical Research Center of Indiana University School of Medicine by using a Roche Cobas Mira S Chemistry analyzer (Roche Diagnostics).

Bone Histomorphometry. For dynamic bone histomorphometric analysis, mice were injected with calcein (30 mg/kg; Sigma) and alizarin red (50 mg/kg; Sigma) 7 and 2 d before killing, respectively, as described (19, 22). Bones were dissected, fixed in 10% buffered formalin, and embedded in methyl methacrylate. Thick (100-μm) cross-sections at the midshaft of the femurs were prepared by using a diamond-embedded wire saw (Histosaw; Delaware Diamond Knives) and ground to a final thickness of approximately 40 μm. Thin (5 μm) longitudinal sections at the medial distal femurs were cut by using a diamond Automated Rotary Microtome Leica RM2255 (Leica Microsystems). Total, single, double, the first and the second labeled perimeter, and interlabel width were measured. A value of 0.1 μm/d was used for mineral apposition rate (MAR) when single labels were present, but double labels were not detected (50). Mineralization lag time (Mlt) was calculated by dividing osteoid thickness by MAR (51). For static bone histomorphometric analysis, longitudinal sections of the distal femurs were stained for TRAPase or von Kossa, and counterstained with Toluidine blue. Histomorphometric analysis was performed by using the OsteoMeasure High Resolution Digital Video System (OsteoMetrics). Total bone volume (mineralized plus osteoid) was used when determining the effect of osteocytic activation of β-catenin on Bone volume per tissue volume (BV/TV) and trabecular parameters. Analyses were performed in the cortical bone at the femoral diaphysis and in the cancellous and cortical bone of an 800-μm region of the distal femur, starting 200 μm below the growth plate. Cortical bone in the distal femur was defined as the bone between the periosteal surface and the endocortical surface derived from the growth plate that continues toward the diaphysis. We cannot exclude the possibility that regions considered as cortical bone contain some trabeculae that formed as outgrowths form the endocortical surface. Osteocyte density was also evaluated in these three regions. Growth plate width was measured in von Kossa/McNeal-stained sections of the distal femur by using the Osteomeasure software. Bone sections were also stained with Goldner's trichrome staining to visualize osteoid and mineralized bone. The terminology and units used are those recommended by the Histomorphometry Nomenclature Committee of the American Society for Bone and Mineral Research (51). The percentage of apoptotic osteoblasts was determined in cancellous bone of the distal femur by staining longitudinal femoral sections with Tdt-mediated dUTP nick-end labeling (TUNEL) kit (EMD Millipore), as published (18).

Immunohistochemistry. The expression of the indicated proteins was visualized in paraffin-embedded femora from 2- and 4-mo-old, as described (17, 18). Briefly, sections were deparaffinized, treated with 3% H_2O_2 to inhibit endogenous peroxidase activity, blocked with rabbit or goat serum, and then incubated with mouse monoclonal anti-CTNNB1 (β-catenin) antibody (1:100; BD Biosciences); rabbit polyclonal anti-Hes1 antibody (1:500; Abcam); goat polyclonal anti-RANKL antibody (1:100; Santa Cruz Biotechnology), or goat polyclonal anti-mouse sclerostin antibody (1:100; R&D Systems). Sections were then incubated with the corresponding biotinylated secondary antibody followed by avidin conjugated peroxidase (Vectastain Elite ABC Kit; Vectora Laboratories). Color was developed with a diaminobenzidine substrate chromogen system (Dako Corp.). Cells expressing the protein of interest are stained in brown, whereas negative cells are green-blue. Corresponding nonimmune IgGs were used as negative controls. The prevalence of sclerostin-positive osteocytes was assessed in cortical bone of the distal femur from 2-mo-old mice.

Quantitative PCR. Total RNA extraction and quantitative PCR (qPCR) were performed as reported (22). Briefly, total RNA was extracted from lumbar vertebrae L4 by using TRIzol (Invitrogen). cDNA was synthesized by using high capacity cDNA reverse transcription kit (Applied Biosystems). Gene expression was analyzed by qPCR using primer probe sets from Applied Biosystems or from Roche Applied Science. Relative mRNA expression levels were normalized to the housekeeping gene ribosomal protein S2 (ChoB) by using the ΔCt method (19, 22).

Western Blotting. Western blotting was performed as described (22). Protein lysates were prepared from femur/tibia diaphysis (~1/3 of the bone). Ten micrograms of protein were separated on a 10% SDS/PAGE and electrotransferred to PVDF membrane (Millipore). Immunoblots were performed by using goat polyclonal anti-mouse β-catenin antibody (1:1,000; R&D Systems), or mouse monoclonal anti-PCNA (1:1,000) or anti-α-tubulinor anti-β-actin (1:2,000) antibodies (Santa Cruz Biotechnology). Blots were developed by using chemiluminescence (Pierce Biotechnology).

Ex Vivo Cultures. Calvarial bones and femora were harvested from 3- and 5-wk-old wild-type animals, and daßcat^{Ot} mice and littermate controls, and maintained in α-MEM containing 10% FBS for 24 h. Bones were then treated with an anti-sclerostin antibody (29) (10 μg/mL; Acris Antibodies) or vehicle for 24 h, and mRNA was isolated. Gene expression was measured by qPCR, as indicated above.

Hematological Measurements. Peripheral blood was collected by tail vein bleeding by using Microvette collection tubes (Sarstedt 20.1278.100), and blood cell count analysis was performed by using the Hemavet machine (Drew Scientific).

Statistical Analysis. Data were analyzed by using SigmaStat (SPSS Science). Differences between control and daßcat^{Ot} mice were evaluated by using Student's *t* test or two-way ANOVA for the comparison of factors age and BMD, as indicated. A *P* value of 0.05 or lower was considered statistically significant. All values are reported as the mean ± SDs.

ACKNOWLEDGMENTS. We thank Dr. Munro Peacock for technical advice and Kevin McAndrews, Meloney Cregor, Hannah M. Davis, Emily Atkinson, Hugo Gabilondo, Amy Sato, and Anthony Acton for technical support and assistance in tissue collection. This research was supported by NIH Grants R01DK076007 and American Recovery and Reinvestment Act Supplement S10-RR023710 (to T.B.), Veterans Affairs Merit Award I01BX002104 (to T.B.), and the Office of Indiana University–Purdue University Indianapolis Vice Chancellor for Research through the Developing Diverse Researchers with InVestigative Expertise program (X.T.). M.M. held short-term visit fellowships from Fundación Conchita Rábago de Jiménez Díaz and the European Molecular Biology Organization.

1. Cauley JA (2013) Public health impact of osteoporosis. *J Gerontol A Biol Sci Med Sci* 68(10):1243–1251.
2. Bonewald LF (2011) The amazing osteocyte. *J Bone Miner Res* 26(2):229–238.
3. Bellido T (2014) Osteocyte-driven bone remodeling. *Calcif Tissue Int* 94(1):25–34.
4. Baron R, Kneissel M (2013) WNT signaling in bone homeostasis and disease: From human mutations to treatments. *Nat Med* 19(2):179–192.
5. Wodarz A, Nusse R (1998) Mechanisms of Wnt signaling in development. *Annu Rev Cell Dev Biol* 14:59–88.
6. Gong Y, et al.; Osteoporosis-Pseudoglioma Syndrome Collaborative Group (2001) LDL receptor-related protein 5 (LRP5) affects bone accrual and eye development. *Cell* 107(4):513–523.
7. Boyden LM, et al. (2002) High bone density due to a mutation in LDL-receptor-related protein 5. *N Engl J Med* 346(20):1513–1521.
8. Little RD, et al. (2002) A mutation in the LDL receptor-related protein 5 gene results in the autosomal dominant high-bone-mass trait. *Am J Hum Genet* 70(1):11–19.
9. Hu H, et al. (2005) Sequential roles of Hedgehog and Wnt signaling in osteoblast development. *Development* 132(1):49–60.
10. Day TF, Guo X, Garrett-Beal L, Yang Y (2005) Wnt/beta-catenin signaling in mesenchymal progenitors controls osteoblast and chondrocyte differentiation during vertebrate skeletogenesis. *Dev Cell* 8(5):739–750.
11. Hill TP, Später D, Taketo MM, Birchmeier W, Hartmann C (2005) Canonical Wnt/beta-catenin signaling prevents osteoblasts from differentiating into chondrocytes. *Dev Cell* 8(5):727–738.
12. Rodda SJ, McMahon AP (2006) Distinct roles for Hedgehog and canonical Wnt signaling in specification, differentiation and maintenance of osteoblast progenitors. *Development* 133(16):3231–3244.

13. Glass DA, 2nd, et al. (2005) Canonical Wnt signaling in differentiated osteoblasts controls osteoclast differentiation. *Dev Cell* 8(5):751–764.
14. Holmen SL, et al. (2005) Essential role of beta-catenin in postnatal bone acquisition. *J Biol Chem* 280(22):21162–21168.
15. Kramer I, et al. (2010) Osteocyte Wnt/beta-catenin signaling is required for normal bone homeostasis. *Mol Cell Biol* 30(12):3071–3085.
16. Kode A, et al. (2014) Leukaemogenesis induced by an activating β-catenin mutation in osteoblasts. *Nature* 506(7487):240–244.
17. Bellido T, et al. (2005) Chronic elevation of parathyroid hormone in mice reduces expression of sclerostin by osteocytes: A novel mechanism for hormonal control of osteoblastogenesis. *Endocrinology* 146(11):4577–4583.
18. O'Brien CA, et al. (2008) Control of bone mass and remodeling by PTH receptor signaling in osteocytes. *PLoS ONE* 3(8):e2942.
19. Rhee Y, et al. (2011) PTH receptor signaling in osteocytes governs periosteal bone formation and intracortical remodeling. *J Bone Miner Res* 26(5):1035–1046.
20. Robling AG, et al. (2008) Mechanical stimulation of bone in vivo reduces osteocyte expression of Sost/sclerostin. *J Biol Chem* 283(9):5866–5875.
21. Robling AG, et al. (2011) Anabolic and catabolic regimens of human parathyroid hormone 1-34 elicit bone- and envelope-specific attenuation of skeletal effects in Sost-deficient mice. *Endocrinology* 152(8):2963–2975.
22. Tu X, et al. (2012) Sost downregulation and local Wnt signaling are required for the osteogenic response to mechanical loading. *Bone* 50(1):209–217.
23. Balemans W, et al. (2002) Identification of a 52 kb deletion downstream of the SOST gene in patients with van Buchem disease. *J Med Genet* 39(2):91–97.
24. Loots GG, et al. (2005) Genomic deletion of a long-range bone enhancer misregulates sclerostin in Van Buchem disease. *Genome Res* 15(7):928–935.
25. Balemans W, et al. (2001) Increased bone density in sclerosteosis is due to the deficiency of a novel secreted protein (SOST). *Hum Mol Genet* 10(5):537–543.
26. Brunkow ME, et al. (2001) Bone dysplasia sclerosteosis results from loss of the SOST gene product, a novel cystine knot-containing protein. *Am J Hum Genet* 68(3): 577–589.
27. Balemans W, et al. (2007) Novel LRP5 missense mutation in a patient with a high bone mass phenotype results in decreased DKK1-mediated inhibition of Wnt signaling. *J Bone Miner Res* 22(5):708–716.
28. Balemans W, et al. (2008) The binding between sclerostin and LRP5 is altered by DKK1 and by high-bone mass LRP5 mutations. *Calcif Tissue Int* 82(6):445–453.
29. Ota K, et al. (2013) Sclerostin is expressed in osteoclasts from aged mice and reduces osteoclast-mediated stimulation of mineralization. *J Cell Biochem* 114(8):1901–1907.
30. Rodilla V, et al. (2009) Jagged1 is the pathological link between Wnt and Notch pathways in colorectal cancer. *Proc Natl Acad Sci USA* 106(15):6315–6320.
31. Estrach S, Ambler CA, Lo Celso C, Hozumi K, Watt FM (2006) Jagged 1 is a beta-catenin target gene required for ectopic hair follicle formation in adult epidermis. *Development* 133(22):4427–4438.
32. Galceran J, Sustmann C, Hsu SC, Folberth S, Grosschedl R (2004) LEF1-mediated regulation of Delta-like1 links Wnt and Notch signaling in somitogenesis. *Genes Dev* 18(22):2718–2723.
33. Hofmann M, et al. (2004) WNT signaling, in synergy with T/TBX6, controls Notch signaling by regulating Dll1 expression in the presomitic mesoderm of mouse embryos. *Genes Dev* 18(22):2712–2717.
34. Chen J, Long F (2013) β-catenin promotes bone formation and suppresses bone resorption in postnatal growing mice. *J Bone Miner Res* 28(5):1160–1169.
35. Javaheri B, et al. (2014) Deletion of a single β-catenin allele in osteocytes abolishes the bone anabolic response to loading. *J Bone Miner Res* 29(3):705–715.
36. Ke HZ, Richards WG, Li X, Ominsky MS (2012) Sclerostin and Dickkopf-1 as therapeutic targets in bone diseases. *Endocr Rev* 33(5):747–783.
37. Wijenayaka AR, et al. (2011) Sclerostin stimulates osteocyte support of osteoclast activity by a RANKL-dependent pathway. *PLoS ONE* 6(10):e25900.
38. Ben-awadh AN, et al. (2014) Parathyroid hormone receptor signaling induces bone resorption in the adult skeleton by directly regulating the RANKL gene in osteocytes. *Endocrinology* 155(8):2797–2809.
39. Rhee Y, et al. (2013) Resorption controls bone anabolism driven by parathyroid hormone (PTH) receptor signaling in osteocytes. *J Biol Chem* 288(41):29809–29820.
40. Rhee Y, et al. (2011) Parathyroid hormone receptor signaling in osteocytes increases the expression of fibroblast growth factor-23 in vitro and in vivo. *Bone* 49(4):636–643.
41. Hilton MJ, et al. (2008) Notch signaling maintains bone marrow mesenchymal progenitors by suppressing osteoblast differentiation. *Nat Med* 14(3):306–314.
42. Tu X, et al. (2012) Physiological notch signaling maintains bone homeostasis via RBPjk and Hey upstream of NFATc1. *PLoS Genet* 8(3):e1002577.
43. Engin F, et al. (2008) Dimorphic effects of Notch signaling in bone homeostasis. *Nat Med* 14(3):299–305.
44. Tao J, et al. (2010) Osteosclerosis owing to Notch gain of function is solely Rbpj-dependent. *J Bone Miner Res* 25(10):2175–2183.
45. Canalis E, Parker K, Feng JQ, Zanotti S (2013) Osteoblast lineage-specific effects of notch activation in the skeleton. *Endocrinology* 154(2):623–634.
46. Stolina M, et al. (2014) Temporal changes in systemic and local expression of bone turnover markers during six months of sclerostin antibody administration to ovariectomized rats. *Bone* 67:305–313.
47. Bivi N, et al. (2012) Cell autonomous requirement of connexin 43 for osteocyte survival: Consequences for endocortical resorption and periosteal bone formation. *J Bone Miner Res* 27(2):374–389.
48. Harada N, et al. (1999) Intestinal polyposis in mice with a dominant stable mutation of the beta-catenin gene. *EMBO J* 18(21):5931–5942.
49. Sakata T, et al. (2004) Skeletal unloading induces resistance to insulin-like growth factor-I (IGF-I) by inhibiting activation of the IGF-I signaling pathways. *J Bone Miner Res* 19(3):436–446.
50. Hauge E, Mosekilde L, Melsen F (1999) Missing observations in bone histomorphometry on osteoporosis: Implications and suggestions for an approach. *Bone* 25(4):389–395.
51. Dempster DW, et al. (2013) Standardized nomenclature, symbols, and units for bone histomorphometry: A 2012 update of the report of the ASBMR Histomorphometry Nomenclature Committee. *J Bone Miner Res* 28(1):2–17.